PERGAMON

Journal of Structural Geology 22 (2000) 1087–1103

JOURNAL OF STRUCTURAL GEOLOGY

www.elsevier.nl/locate/jstrugeo

Deformation structures and implications for fluid flow at the Costa Rica convergent margin, ODP Sites 1040 and 1043, Leg 170

Paola Vannucchi [a,*], Harold Tobin [b]

[a] *Dipartimento di Scienze della Terra, Università di Modena, Piazzale S. Eufemia, 19, Modena, Italy*
[b] *Department of Earth and Environmental Sciences, New Mexico Institute of Mining and Technology, Socorro, NM 87801, USA*

Received 17 November 1998; accepted 21 March 2000

Abstract

During ODP Leg 170, five sites were drilled and sampled off the Costa Rica Pacific margin. Two of them, site 1040 and 1043, yielded material from a wedge of deformed sediments, the main décollement zone, and the underthrusting sedimentary sequence of the subducting Cocos plate. Detailed mesoscopic and microscopic analyses of the deformation features characteristic of each domain help to define four different structural/hydrologic regimes. Unexpectedly, the wedge of deformed hemipelagic sediments does not represent an accretionary wedge, because little or no transfer of material from the subducting plate has occurred. The deformed sedimentary wedge records periods of tectonic bulk strain, in which fluid pressure intermittently rises and induces fracturing, alternating with periods of gravitational bulk strain. The last stage of this alternating strain regime is represented by the growth of thick, sub-horizontal shear zones. The sediments caught up in the décollement zone show distinctly different deformation features, reflecting different mechanical behaviour and a different response to fluid flow, but again transient pulses of increased pore pressure are interpreted as the driving mechanism of dewatering. The underthrust pelagic and hemipelagic section is also characterised by dewatering features, but only in the uppermost part. The basal sediments of this section, in contact with underlying gabbro intrusions, have a completely different structural history and hydrologic regime. Structures here are interpreted as related to near ridge processes, and the hydrologic system is not linked to the upper sediment-dewatering regime, but rather seems to have been fed by a seawater source.

1. Introduction

The processes that take place in the evolution of convergent margins, from oceanic subduction to orogenic belt, are now reasonably well known, although the observations are concentrated on land and mainly at a regional scale. The exploration of active oceanic margins below sea level presents logistical problems, but it is essential to the understanding of the whole system. Scientific drilling in the Barbados and Nankai accretionary prisms, for example, has been of primary importance in establishing the fold-and-thrust architecture and the deformational behaviour and mechanical properties of wedge sediments. These two locations are also the first two where an active décollement zone has been drilled into and studied.

ODP Leg 170 was focused on the Costa Rica active margin, where the Cocos plate is subducted beneath the Caribbean plate (Fig. 1). Reasons for drilling this particular margin included the need to establish the relative importance of sediment offscraping, underplating and subduction erosion (Shipley et al., 1992; Hinz et al., 1996) as forearc tectonic processes. The absence of trench deposits leads to a clear signal of dewatering and a record of the degree of sediment subduction, so that the Costa Rica margin is an ideal location to address long standing problems of subduction zone mass balance and sediment recycling to the mantle

* Corresponding author.
E-mail address: paolav@geo.unifi.it (P. Vannucchi).

0191-8141/00/$ - see front matter
PII: S0191-8141(00)00027-4

(Scholl et al., 1994; Kimura et al., 1997). This margin is also one of the few where carbonates are actively being subducted.

The objective of this paper is to investigate the relationship between deformation, dewatering and fluid flow in three different parts of the margin: the deformed sedimentary wedge, the décollement zone, and the underthrust section. The approaches used include core-scale and optical and scanning electron microscope examination of structures, together with laboratory results on the relationship between deformation, permeability and pore water geochemistry.

2. Tectonic setting of sites

At the Costa Rica margin, the Cocos and Caribbean plates are converging at about 8–9 cm/y (Von Huene et al., 1995). The subduction vector is approximately perpendicular to the margin (Fig. 1). Off the Nicoya Peninsula, where Leg 170 was located, ocean floor morphology is generally smooth, with no seamounts or ridges being subducted.

Leg 170 consisted of five sites (Fig. 1): one reference site on the undeformed Cocos plate (Site 1039), two sites in the lower slope (Sites 1040 and 1043) and two sites in the mid-slope (Sites 1041 and 1042). Our attention is here focused on sites 1040 and 1043. These two sites were chosen to pass through the toe-lower slope sediments (here referred to as the deformed sedimentary wedge), the décollement, and the underthrust section to reach the Cocos plate oceanic crust (Fig. 2). Comparisons between the underthrust section and the reference site are also presented.

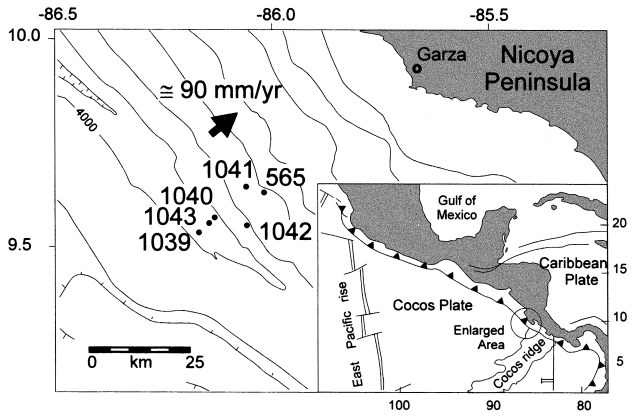

Fig. 1. Locations of Leg 170 sites and Leg 84 site 565 off Nicoya Peninsula. The plate convergence vector (Von Huene et al., 1995) and the smooth morphology of the Cocos plate are shown. The box shows a simplified tectonic sketch of Central America.

3. Large scale structure of the margin

At the Costa Rica margin, the balance among sediment accretion, sediment subduction and subduction erosion of the forearc is poorly understood. Prior to drilling, the seismically imaged wedge of deformed sediments of the lowermost trench slope (Fig. 2) was believed to be a small accretionary prism of sediment scraped off the downgoing Cocos plate (e.g. Shipley et al., 1992; McAdoo et al., 1996). However, reflector tracing of the underthrusting sedimentary package had indicated that relatively little of the incoming section was being frontally accreted (Shipley et al., 1992).

Drilling results from sites 1043 and 1040 clearly show that the material making up the sediment wedge is stratigraphically distinct from all the units cored at the site 1039 reference section (Kimura et al., 1997; Fig. 2). The deformed sediment wedge consists of rather homogeneous hemipelagic sediments, essentially all silty clays and sedimentary breccias with silty clay forming the clasts and the matrix. These sediments are fossil-poor, whereas even the uppermost sediments at the reference site (1039) are diatom-rich. Marked differences in trace-element chemistry also distinguish these two sections. This evidence shows that accretionary transfer through offscraping has not occurred, consistent with the observation that the full incoming section is present beneath the décollement zone (Fig. 2). For this reason, we have chosen not to refer to this wedge as 'accretionary' but simply as 'deformed'. The lithology and chemistry of the deformed wedge indicate terrestrial, arc-derived sediments, and the presence of sedimentary breccias, midslope fossil assemblages and lack of trench turbidites all imply mechanical mixing of material during downslope transport to the base of the continental slope, rather than frontal accretion (Kimura et al., 1997). Seismic reflection data and macroscopic structural observations in this domain are consistent with thrusting deformation in a compressional tectonic regime with mass added from upslope by slumping and debris flows (Kimura et al., 1997).

The backstop to the deformed sedimentary wedge is formed by the landward-dipping boundary of the margin basement seismic unit (Fig. 2). Based on seismic velocity and reflective character the latter is either ophiolitic material similar to the onshore Nicoya complex or well-lithified Mesozoic accreted material. This margin basement is overlain by a 300–600-m-thick slope blanket of hemipelagic sediment, termed the slope apron and cored at sites 1041 and 1042. The boundary between the slope apron and the sedimentary wedge is seismically indistinct, and the sediment types are similar. Hence the deformed sedimentary wedge is interpreted as predominantly a deformed counterpart to the apron, perhaps with more extensive downslope transport.

The Cocos plate sedimentary sequence is underthrust in its entirety beneath the sedimentary wedge at least as far landward as site 1040. This sequence, which is affected by normal faulting rooted in the oceanic basement, is rapidly compacted as it is underthrust, as seen in the dramatic thinning of reflector sequences (Shipley et al., 1992) and documented by logging and porosity data from the drilled transect (Kimura et al., 1997). The presence of small, predominantly reverse faults and steep bedding dips, coupled with seismic interpretation, suggest incipient thrusting may cut the sequence at the base of Unit U2 (Fig. 2). Overall, however, the section below the décollement zone is deformed primarily by vertical compaction as it is carried beneath the sedimentary wedge. The present tectonic regime of the margin is hence one of no

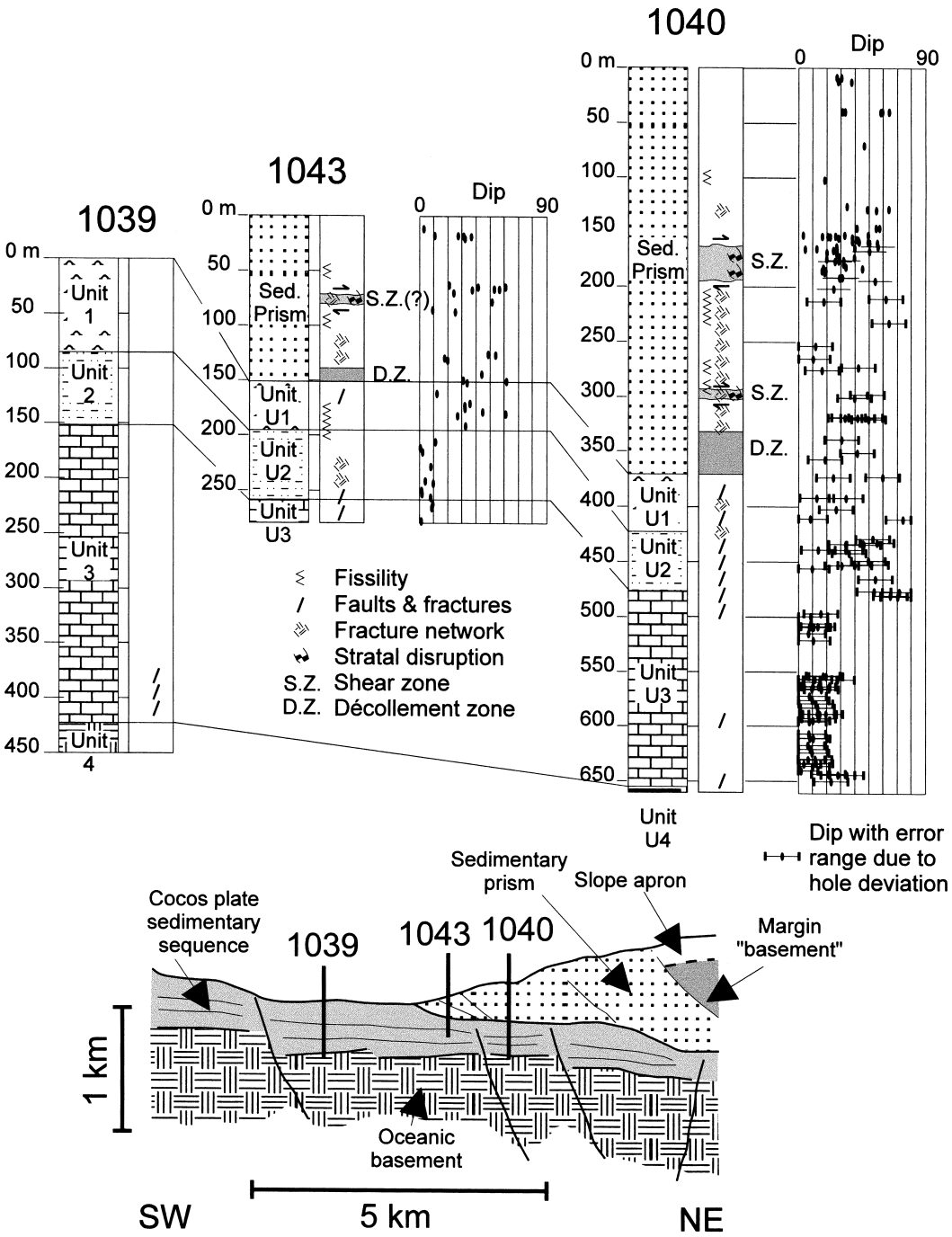

Fig. 2. Lower slope section from the seismic line by Shipley et al. (1992) with sites 1039, 1043 and 1040 locations. For each site the lithostratigraphic column is presented and a summary of the principal deformation features detected at the meso-scale. The thickness comparison between site 1039 units and site 1040 underthrust section is also illustrated (see text for the unit descriptions).

accretionary offscraping. Either complete subduction or active tectonic erosion may be occurring, or alternatively, accretion solely by underplating further landward may be taking place. The drilling results and other data available cannot yet discriminate between these possibilities.

4. Sites 1040 and 1043

4.1. Sedimentary wedge

4.1.1. Core-scale observations

Drilling at sites 1040 and 1043 penetrated the entire wedge and intersected sediments above the décollement for 371.2 and 150.57 m, respectively. The recovered material is very similar at the two sites and is composed of clay(stone) and silty clay(stone) (Kimura et al., 1997) deposited by turbidity currents and debris flows. The age has been estimated to be Pliocene–Pleistocene (Kimura et al., 1997).

As reported in Kimura et al. (1997), deformation in the deformed sedimentary wedge is indicated by inclined bedding, fissility, core-scale faults with small (0.5–1 cm) offsets, fracture networks, brittle–ductile stratal disruption, deformation bands and incipient scaly fabric (see Lundberg and Moore, 1986, and Maltman, 1998, for discussion and terminology). Microfaults are uncommon, but fracture networks of varying intensity are scattered over the entire section (Fig. 2). Fissility is concentrated in intervals, as shown in Fig. 2, as are small deformation bands and pinch-and-swell structures. Pore-water geochemical data (especially chlorinity), porosity and the micropalaeontological record all change abruptly at specific depths (Kimura et al., 1997), indicating possible fault-based fluid conduits; these breaks, however, are not always marked by observed shear zones. Toward the base of the sedimentary wedge, the amount of fracturing gradually increases and the boundary with the top of the décollement zone is somewhat arbitrarily placed at the first occurrence of fractures with polished surfaces, typical of incipient scaly fabric.

4.1.2. Microscopic observations

Bioturbation and pellets are common throughout the sedimentary wedge. Numerous escape tracks testify to the occurrence of episodes of high sedimentation rate. SEM observations on undeformed sediments from the topmost 80 m of the section show high porosity, with very weak preferred orientation of clay minerals. With increasing depth beyond 80 m below sea floor (mbsf), clay mineral orientation is progressively enhanced. This clay mineral orientation is attributed to gravity-induced compaction as depth is the only parameter that varies among these samples. Logging While Drilling (LWD) measurements (Kimura et al., 1997) show that averaged porosity decreases from 65% to 55% and bulk density increases from 1.6 g/cm^3 to 1.8 g/cm^3, in correspondence with microscopic observations. Silt is abundant and occurs in small, uncemented lenses or laminae, providing inhomogeneity at the microscopic scale.

Three types of deformation structures dominate: kink-like bands, deformation bands and small, thin faults. Kink-like bands are sharp deflections of the primary sedimentary fabric, as described by Lundberg and Moore (1986) and Maltman et al. (1993) for the Nankai accretionary prism. Deformation band is a general term that is used here to describe planar zones within which clay minerals are aligned sub-parallel to the edges, such that they maintain a distinct ductile appearance at the microscopic scale. Faults are brittle, discrete structures showing displacement.

Cross-cutting relationships show that kink-like bands are the oldest structures. They are neither abundant nor well developed, and were not recognised at the core scale. They appear at site 1040 in samples from below 150 mbsf. They are commonly less than 0.5 mm wide and vary in thickness along their length (Fig. 3).

These kink-like bands are commonly developed where clay mineral preferred orientation is well developed (Fig. 3), and are typically oriented at high angles to the plane of clay mineral preferred orientation (between 40° and 70°). They form conjugate sets symmetrically disposed around the perpendicular to the clay mineral preferred orientation with a dihedral angle that ranges from 70° to 90°. Where marker horizons are present, the offset on the kink-bands is small (less than a millimetre) and commonly of reverse sense, with a few of normal sense. Kink-like bands here are too narrow and poorly developed to permit detailed description of associated substructures.

Geometrical analysis of the limited data-set of kink-like bands, following Suppe (1985) and Byrne et al. (1993), show that they have rather high external angles (between 40° and 55°), while internal angles are around 40–50°. They are thus similar to those at the Nankai Trough (ODP Site 808, Byrne et al., 1993) and indicative of a decrease in sediment volume. They are interpreted as consolidation-induced features. Consolidation took place in the sedimentary wedge both by homogeneous porosity loss, as LWD data implies, and by production of discrete kink-like bands. At site 1040 at depths below 150 mbsf, porosity is around 45–50%, decreasing to an average of 40% at 200 mbsf. The porosity for a given depth of burial in the Costa Rica sedimentary wedge corresponds generally to normal consolidation with intervals of overconsolidation, such as the macroscopic shear zones (Bolton et al., 1999). These results are in line with the porosity necessary for

kink development and support experimental tests showing that shearing in normally consolidated sediments causes a volume loss to achieve critical state (Bolton et al., 1998).

Deformation bands displace kink-like bands and are the most common deformation features in the whole sedimentary wedge. They are particularly concentrated in site 1040 macroscopic shear zones, where they can be up to 5 cm long and 2 mm wide.

The internal structure of deformation bands is always characterised by a strong alignment of clay minerals parallel to the edge (Fig. 4). The deformation bands contain very thin, small clay particles that tend to cluster around and between larger domains and particles. The orientation of these small clay particles is parallel to the deformation band's edges. This phenomenon implies intergrown domains (Smart and Tovey, 1981). The X-EDS spectrum of the intergrown domains shows significant iron and manganese enrichment together with depletion in both aluminium and silicon. The intergrown domains have been identified, in line with Schoonmaker et al. (1985) and Dadey et al. (1990), as authigenic smectites. Thus the deformation bands contain both detrital and authigenic smectites.

Two types of deformation bands have been distinguished on the basis of geometry and morphology: swarms forming a network-like pattern and single, thick shear bands (Fig. 4). The network comprises intersecting, mutually cross-cutting bedding-parallel and bedding-oblique bands (Fig. 4). The bedding-parallel bands are commonly about 0.1 mm wide and 1 cm long and are usually better formed than the bedding-oblique bands, which are typically about 0.01 mm wide and 0.5 mm long. Generally the network bands show some displacement: usually reverse for bedding-parallel bands and normal for bedding-oblique bands (Fig. 4). Complex but systematic mutual cross-cutting relationships suggest several episodes of deformation band development. A general trend is observed of progressive increase of the width of the bands with age, so that the older bands are thicker than the younger ones.

Discrete, fabric-parallel, low-angle, thick (>1 mm) deformation bands recording shear cut the networks of narrow deformation bands (Fig. 4). The thick deformation bands often exhibit a shear-zone geometry in thin section, with straight bands defining the margins at the top and the bottom, and sigmoidal or secondary bands in between (Fig. 4). Secondary surfaces are not

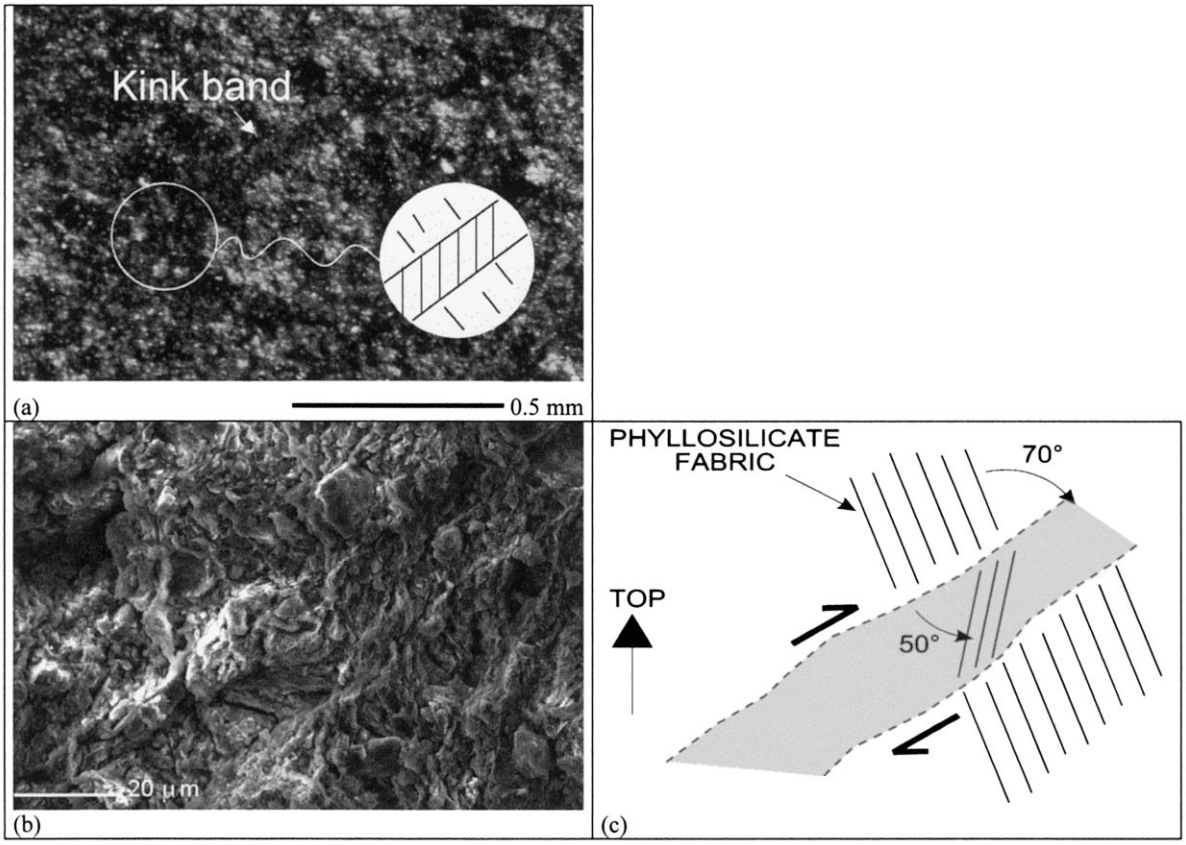

Fig. 3. Deformed sedimentary prism: (a) Detail of kink band (sample from 103.84 mbsf, Site 1040). (b) Secondary SEM image showing a kink-band (sample from 92.34 mbsf, site 1040). (c) Line drawing of (b) with the external and internal angles measured for the kink-band.

always present. If present, Y, R and R_2 (Logan et al., 1979; Teas et al., 1995) are well developed, providing shear sense indicators.

Below 200 mbsf at site 1040 there are areas where deformation bands are so numerous that the sediment has two preferred clay mineral orientations, one due to the bedding fabric and the other due to the shear zone bands. The well-developed phyllosilicate fabric of the shear zone bands suggests a substantial porosity and volume loss relative to the surrounding sediments.

In contrast to the deformation bands, faults are narrow and discrete, characterised by a dark, reddish colour (Fig. 5). They occur as later features, cutting all previously described structures. Faults develop as rectilinear features, typically less than 0.01 mm wide and less than 1 cm long, and are commonly arranged en échelon (Fig. 5). In contrast, faults in the underthrust section are anastomosing. Faults occur in conjugate sets oriented obliquely to the clay mineral preferred orientation (Fig. 5) and form a wide spectrum of dihedral angles. SEM observations show that fault surfaces are variably polished and commonly lineated. Movement indicators are rare, but reverse movement is most common, followed by strike-slip and then normal. Fig. 6 shows the deformation features observed at different depth levels.

SEM analyses show authigenic barite crystals in the two shear zones identified at site 1040. Barite was also found in cores from the décollement of the Barbados accretionary prism and interpreted as evidence of deposition by flow of exogenous fluid (Shipley et al., 1995).

4.1.3. Kinematic model of sedimentary wedge deformation

Compacted but otherwise undeformed sediments show a clay mineral fabric parallel to bedding, indicating gravity consolidation occurred early in the sedimentary wedge history, inducing mineral reorientation and porosity loss.

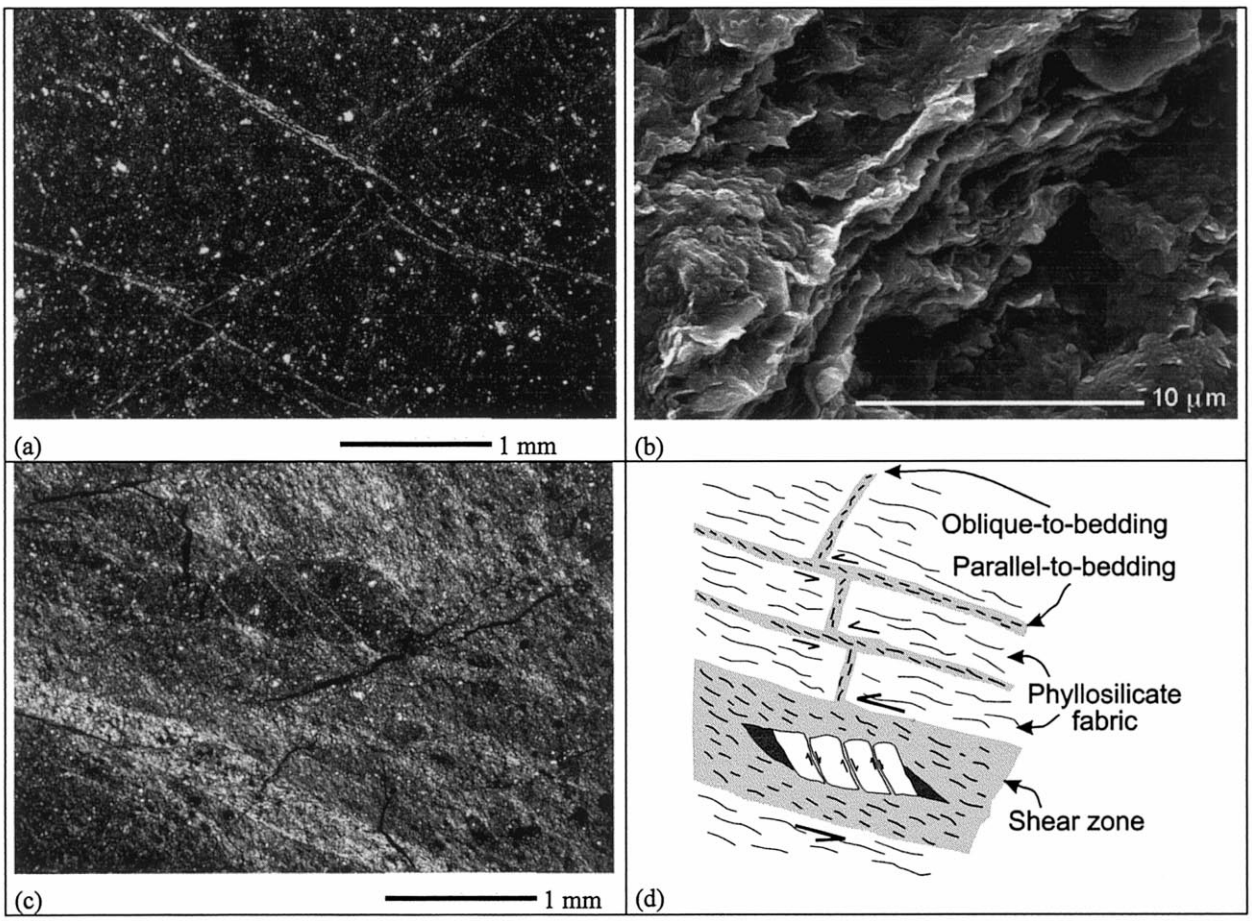

Fig. 4. Deformed sedimentary wedge: (a) Photo-micrograph of an example of bedding-parallel and bedding-oblique networks (also illustrated in d) (sample from 169.47 mbsf, site 1040). (b) Secondary SEM image showing a deformation band of the bedding-oblique system (sample from 185.06 mbsf, site 1040). (c) Micrograph of a thick shear band with fragmented blocks showing a domino-like fault system, used to determine the sense of shearing (sinistral) (sample from 185.06 mbsf, site 1040). (d) Sketch of the deformation band relationships relative to the phyllosilicate fabric as shown in (a) and (c).

Kink-like bands record the initial collapse and densification of the sediments resulting in a volume decrease. In the Costa Rica sedimentary wedge, geometry and sense of movement of kink-like bands demonstrate that they are related both to bedding-perpendicular and bedding-parallel compression (Fig. 6). The orientation and the wide dihedral angle of conjugate kink-like bands (up to 90°) imply bulk lateral shortening at an internal angle of friction approaching 0°. Whether this shortening is due to tectonic stress or gravitational collapse is unclear.

Deformation continued with the development of deformation bands, in which the realignment/flattening of clay minerals is more efficient and can be achieved by two very different processes: shearing or porosity collapse. These two mechanisms are implied by the presence of secondary shear surfaces and shear sense indicators, and by the inhomogeneous densification of the sediments, observed both in thin sections and through physical property data.

Deformation band development by shearing may occur through a further evolution of kink-bands, as suggested in Maltman et al. (1993), who interpreted the progressive rotation and increased preferred orientation of clay minerals as the result of increasing strain. Experimental work (Bolton et al., 1998) demonstrates that shearing can allow partial realignment only for a limited thickness. On the other hand, in the evolution from kink to deformation band, there is a volume decrease, produced by a porosity decrease, and water release (Maltman et al., 1993; Bolton et al., 1998).

In the second possible scenario, deformation bands may be the direct expression of high pore pressure in the sediments. The fluid overpressure induces local dilation during shear and the development of dewatering channels. The eventual collapse of the channels results in densification of clay-rich zones. The presence of authigenic smectites in the deformation bands attests to fluid flow. These observations are in line with the physical property results and the geomechanical behaviour observed in experiments (Bolton et al., 1999).

We suggest that a combination of the shear and collapse processes produced flattening in two, sub-perpendicular orientations giving rise to the swarms of network deformation bands. According to critical state theory (Jones and Addis, 1986, Bolton et al., 1998), and geomechanical properties of site 1040 samples measured in the laboratory (Bolton et al., 1999), normally consolidated material loses volume during shearing (Bray and Karig, 1985). Bedding-parallel and bedding-oblique bands thus result from similar processes, but differences in the observed alignment of particles in these mud-rich sediments implies different effective stress conditions. The intensely aligned particles of bedding-parallel bands, constrained within narrow horizons, represent slip under condition of reduced effective stress (Bolton et al., 1998). Consolidation followed by effective stress reduction causes sediments undergoing shear to increase in porosity, dilate, and then collapse, resulting in an overconsolidated state (Bolton and Maltman, 1998).

The geometry of the deformation band network, and its complex mutual cross-cutting relationships, suggest that the bedding-oblique and bedding-parallel bands formed under alternating strain regimes where bedding-parallel/horizontal and bedding-perpendicular/vertical strains dominated (Fig. 6). We interpret the vertical strain as being associated with burial and increasing gravitational load with increasing depth in the sedimentary wedge. Either gravitational loading due to lateral extension, or tectonic stress might have induced the horizontal strain. The presence of at least one major, and seismically imaged, shear zone at site

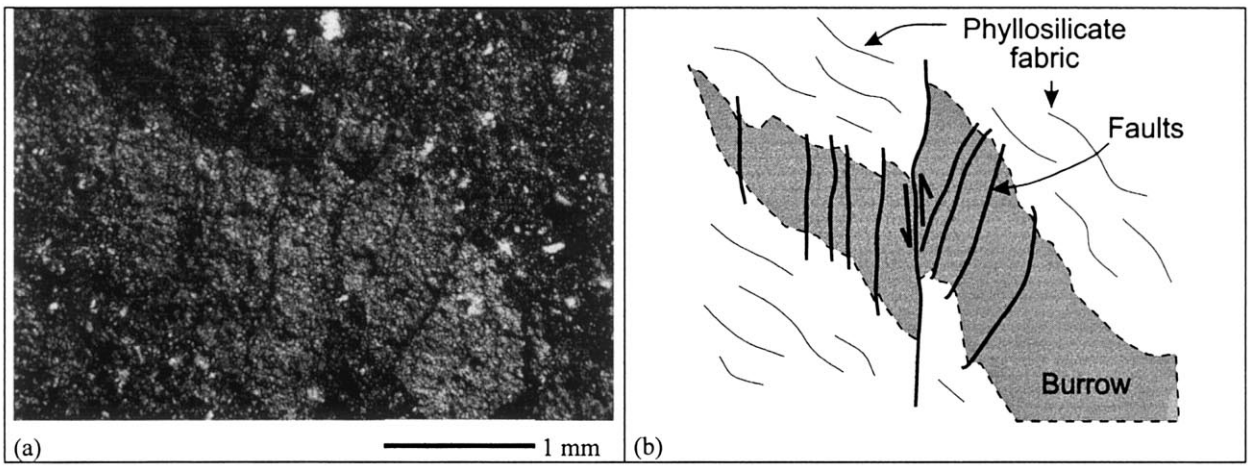

Fig. 5. Deformed sedimentary wedge: (a) Micrograph showing a faulted burrow. The faults are organised en échelon (sample from 176.65 mbsf, site 1040). (b) Line drawing of (a) showing the offsets.

1040, and the regular downward progression of structures from vertical to horizontal shortening, argue for the presence of active tectonic compression in the sedimentary wedge.

Further development of shear deformation bands is the expression of the establishment of a steady-state bedding-parallel strain. With depth, the sedimentary wedge deformation bands become more common and their spacing decreases, culminating in an apparently pervasive foliation at 335–350 mbsf. This implies that the deformation has a tendency to evolve from discrete to continuous (Fig. 6).

As demonstrated by experimental work (Byrne et al., 1993; Bolton et al., 1998), deformation bands are barriers to fluid flow, because permeability decreases with progressive development of the structures, except during transient pulses of high pore pressure. Development of high pore pressure is likely here due to the consolidation occurring through porosity collapse, to the clay-rich nature of the sediments, to the resulting inhibition of permeability, to experimental data showing these sediments lose porosity and dewater at a rate low enough to produce overpressure (Bolton et al., 1999). One can envisage that the greater the number of deformation bands that develop in the sediments, the more the pore pressure rises locally, inducing new formation of deformation bands. This positive feedback might proceed until dewatering removes the possibility of further pore-pressure increase.

Triaxial test data also show that macroscopic shear

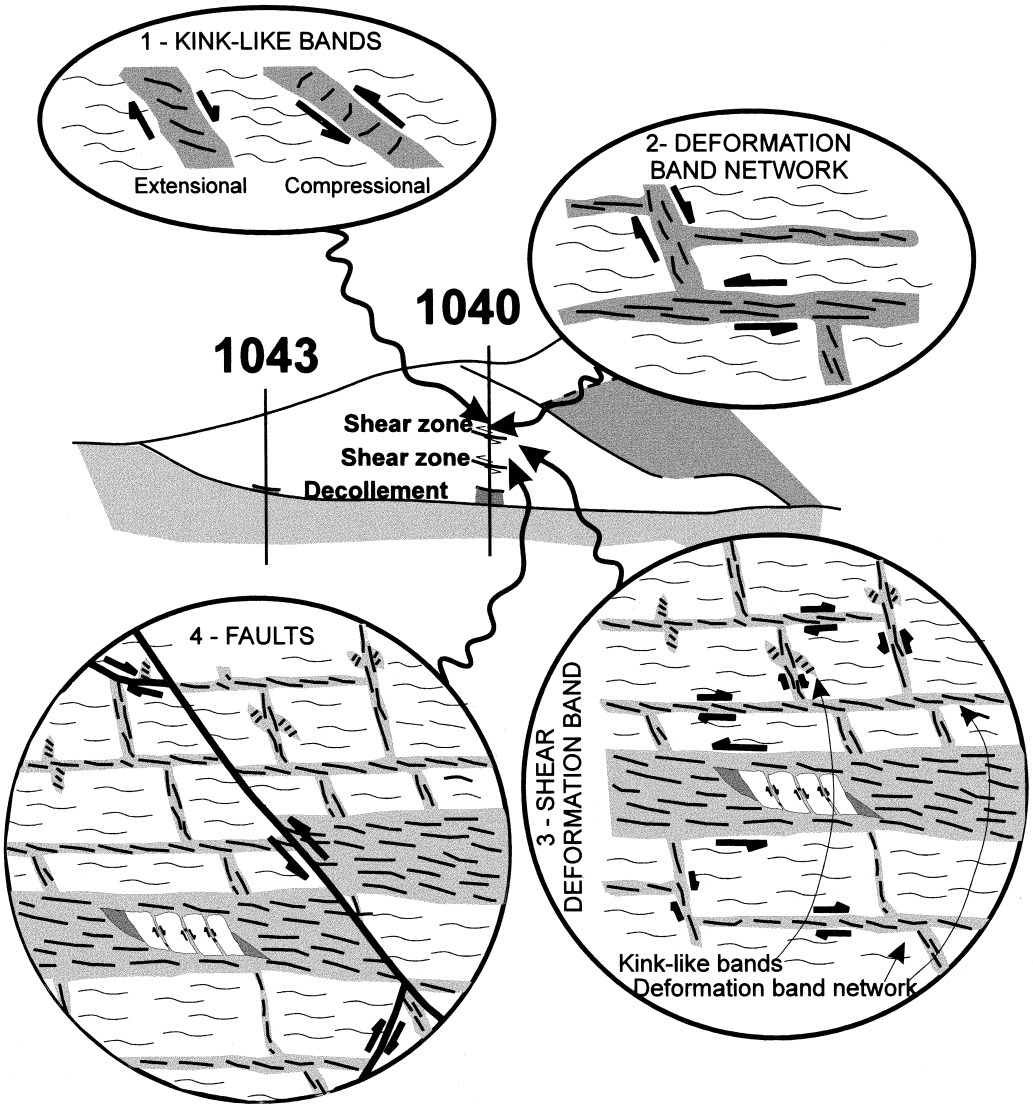

Fig. 6. Sketch of the deformed sedimentary wedge deformation history as detected through microstructural analyses. Shaded areas are zones of reoriented phyllosilicate. The network implies transient and episodic dewatering, followed by development of shear zones. The entire deformation band process drives the sediment to progressive consolidation producing areas of relatively high consolidation (see the 'clay pod' in the shear band of Fig. 4b).

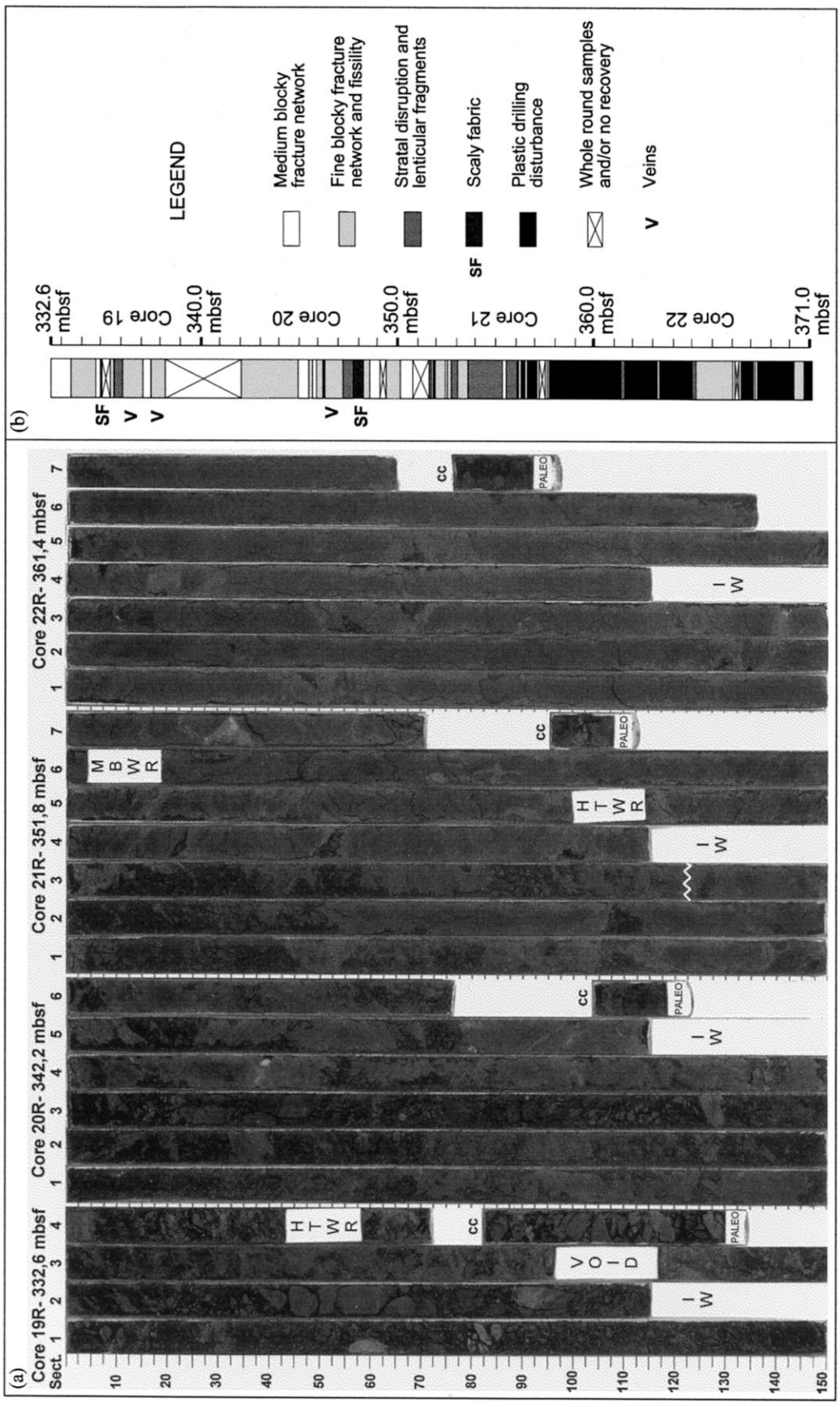

Fig. 7. (a) Image of all the décollement cores from site 1040 (sections and core catchers—cc). The white zigzag line marks the limit between the upper brittle and the lower plastic part. IW, HTWR and MBWR are location of whole round samples. (b) Structural log of the same interval.

zones, where the geochemical analysis of pore water identified fluid flow channels (Kimura et al., 1997) and where structural investigations found a major concentration of deformation bands, are overconsolidated (Kimura et al., 1997; Bolton et al., 1999). Dilation and the occurrence of real channels in the macroscopic shear zones shows that these horizons are the most effective fluid conduits in the wedge.

The latest deformation of the densified sediment takes place by faulting (Fig. 6), which we interpret as marking a stage where the sedimentary wedge has reached an overconsolidated brittle state. The deformation features in the deformed sedimentary wedge thus record clearly a non-steady state stress regime, in which tectonic and gravitational stresses compete and are perhaps modulated by time-varying pore pressure, leading ultimately to a brittle behaviour as the sediments progressively compact.

4.2. Décollement zone

4.2.1. Core-scale observations

The décollement zone is the physical detachment between the subducted and the overriding plates. In the cores from both sites 1040 and 1043, it was clearly identified by structural features, although other parameters, such as physical properties, LWD data, micropalaeontology, and pore fluid geochemistry, also record significant changes in the same interval (Kimura et al., 1997).

Mesoscopically the décollement zone is highly heterogeneous with respect to the distribution of brittle and ductile deformation (Fig. 7). In both the 9-m-thick décollement zone at site 1043 and the 38.6-m-thick zone at site 1040, however, it is possible to subdivide the décollement into two domains: a brittle upper and a ductile lower domain (Fig. 7). At site 1040, where the recovery of core was good, the brittle domain is 24.2 m thick and the ductile one is 14.4 m thick.

In the brittle domain, fracture networks break cores into lenticular to blocky fragments on the millimetre to centimetre scale. The most disrupted sediments exhibit anastomosing discontinuous and interpenetrative fractures. Fig. 7 shows the alternation of fracture networks and anastomosing fractures through all the recovered core of the brittle domain. Some fracture surfaces are polished. Two thin intervals of incipient scaly fabric have been recovered, but nowhere is it fully developed (Fig. 7). Several millimetre-scale veinlets filled with calcite and rhodochrosite were also present. The presently ductile domain is formed by soft, plastic silty clay, which was unfortunately intensely deformed by the drilling process, prohibiting structural study (Kimura et al., 1997). The fact that these two domains had such different responses to coring suggests they have quite distinct in-situ rheology.

4.2.2. Microscopic observations

Microscopic observations have been carried out on site 1040 samples down to the boundary between the brittle and the ductile regime (356 mbsf) where the intense drilling disturbance begins. SEM observations of samples from the brittle domain indicate a high level of heterogeneity in the grain size of the sediments, in the deformation style (Fig. 8a), and in the clay mineral fabric (Fig. 8b, c).

Silt is occurring in laminae or lenses surrounded by clayey material. Silt and clay are generally well separated. In the clayey material, areas of poorly oriented clay minerals, generally characterised by a high percentage of smectite (Fig. 8b) and incipient carbonate cementation (Fig. 8c) as documented by SEM and X-ray analysis, alternate with areas of well developed preferred orientation. The areas of poorly oriented clay minerals can have either high or low porosity. Cementation in silty areas varies from absent to incipient, but smectite authigenesis is locally well developed (Fig. 8b).

Irregular and discontinuous sets of fractures and deformation bands surround zones of relatively undeformed, cemented clay defining a domainal texture (Fig. 8c). These little-deformed domains are detectable at the core scale in the uppermost part, but are microscopic at the boundary between the brittle and the ductile parts of the décollement. Thus the deformation style is domainal through the entire brittle upper part of the décollement zone, but the size of the domains decreases downwards through the décollement zone. This deformation style resembles hydraulic brecciation and shows that brittle deformation is visible even at the SEM scale of observation (Fig. 8b). The domains are more evident in the clayey material, where they are separated by irregular deformation bands, ranging from thin and discontinuous to anastomosing and slightly thicker. Networks of deformation bands here are thinner than those in the deformed sedimentary wedge. The intense preferred orientation of clay minerals within the bands suggests a high component of flattening accompanying shear.

Shear deformation bands, similar to those described in the deformed sedimentary wedge, are also present. These cut the domainal texture (Fig. 8a, d). The relationships between the network and the shear deformation bands are here less clear, but mutual cross-cutting of each type of deformation band suggests episodic formation. Incipient scaly fabric is developed in slightly cemented clay-rich horizons (Fig. 8e). At the microscale, incipient scaly fabric is characterised by lineated surfaces, not always polished, that are distributed discontinuously in the sediment. Apart from the lineations, there is no other evidence of shearing in the sediment affected by incipient scaly fabric (Fig. 8e).

Euhedral rhodochrosite crystals occur in small

aggregates (Fig. 8d). A clear vein-like morphology is not visible in the examined samples, even though a few veins were noted during mesoscale observations (Kimura et al., 1997) (Fig. 7). Patches of rhodochrosite crystals were also recovered in samples from the disturbed lower part of the décollement zone.

4.2.3. Kinematic model of décollement deformation

The dewatering and deformational history of the décollement appears to be less systematic than that of the overlying wedge. Here the association of microstructures suggests the variable presence of high porosity zones and low porosity zones (Fig. 9). High

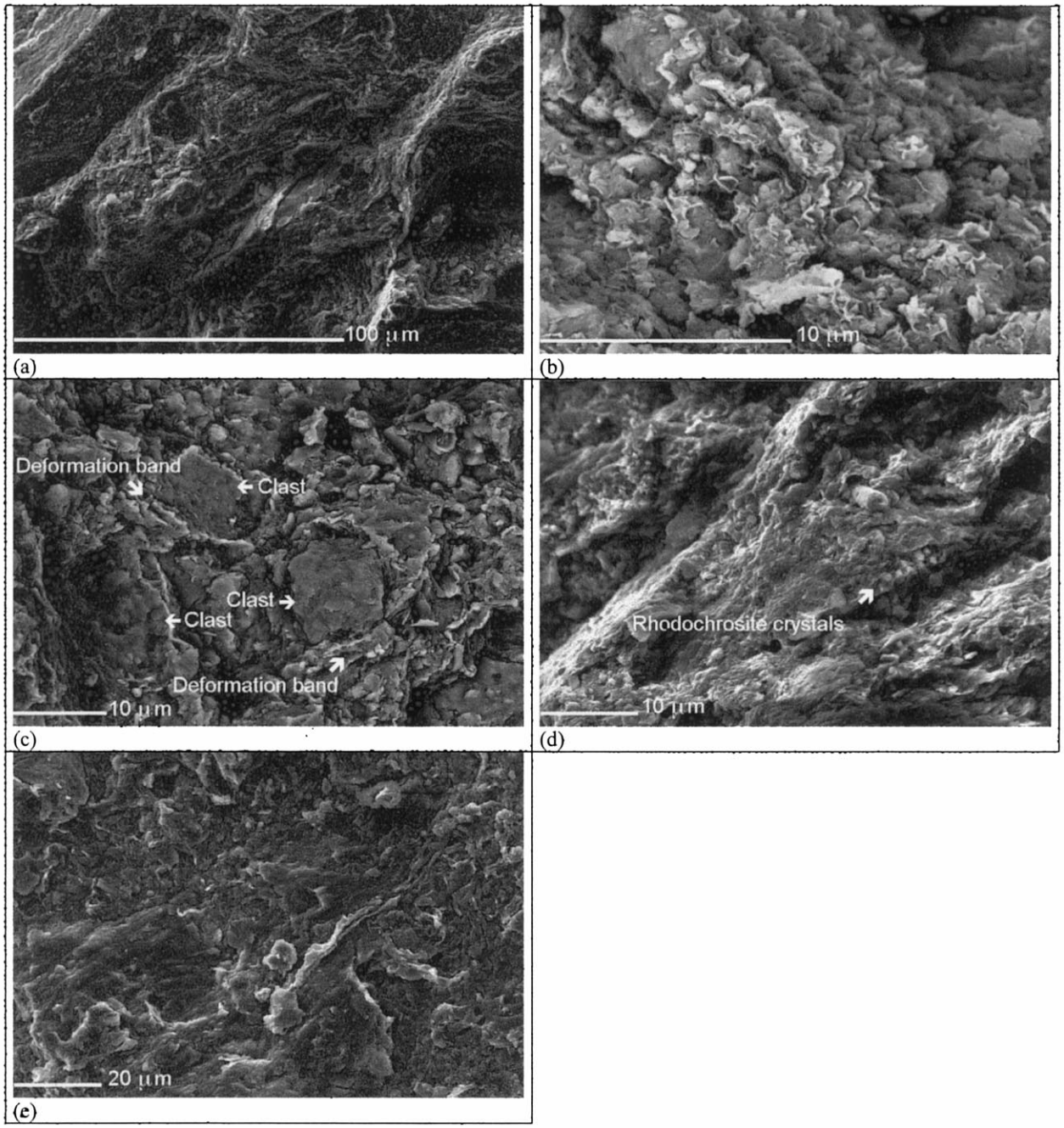

Fig. 8. (a) Secondary SEM image showing the general features of the sediment in the décollement zone, exhibiting alternation of brittle and ductile deformation features. (b) Backscattered SEM image of a silty lens with authigenic smectite. (c) Secondary SEM image of the breccia-like texture. (d) Backscattered SEM image of a shear zone with a patch of rhodochrosite crystals. (e) Secondary SEM image of incipient scaly fabric surfaces.

porosity zones are silty, allowing diffusive flow, and lack evidence of shear. Low porosity zones may be either silt or clay dominated. The low porosity silty zones are the products of smectite authigenesis and slight cementation, both secondary phenomena that imply the presence of earlier diffusive flow and the lack of shear. Clayey low porosity zones show that collapse and authigenesis occurred in zones dominated by channelised flow. The pervasive arrangement of deformation bands argues for multiple small openings followed by collapse. Each channel represents a barrier to fluid flow, and new overpressure at higher strain values is required. We interpret the general regime to be episodic strain with transient overpressure. Evidence of both flattening and shearing is present. Euhedral calcite and rhodochrosite crystals, occurring as little pockets in clay-rich horizons, suggest exogenous fluid influx through these carbonate-poor sediments.

The influence of diffusive flow in the décollement circulation is minor due to the isolation of the silty areas and the lack of communication among them (Fig. 9). Their presence and distribution may play a role, however, in enhancing the heterogeneity of the décollement and locally they could act as storage areas for fluids. Pore-water accumulation in these areas, together with tectonic compression, might intensify dewatering through the clays.

Deformation bands are again the most common deformational features in clayey areas. Compared with the deformed sedimentary wedge fabric, collapse in the décollement zone produced much narrower, yet more widely distributed, deformation bands throughout the zone. This deformation style implies that décollement dewatering occurred through many small transient pore pressure fluctuations, which may be large enough to open channels. Shearing, acting on discontinuities, may help the channel become active, and as long as the channel remains open, it is easy for shear to be concentrated there. The process is thus kept active through a positive feedback.

We interpret that deformation bands in the décollement zone are produced through hydraulic brecciation. In fact, cemented or well-compacted material is broken, causing brecciation and collapsed phyllosilicate frameworks between individual shear surfaces (Fig. 9). On the other hand, the slight cementation prohibits the development of a fully pervasive scaliness, resulting in an incipient scaly fabric. Hydraulic brecciation implies hydrofracturing and supports the hypothesis of at least episodically high fluid pressure.

The co-occurrence of deformation bands and hydraulic breccia (Fig. 9) suggests that the décollement zone is a zone of spatial and/or temporal variability in terms of fluid pressure and deviatoric stress. The dewa-

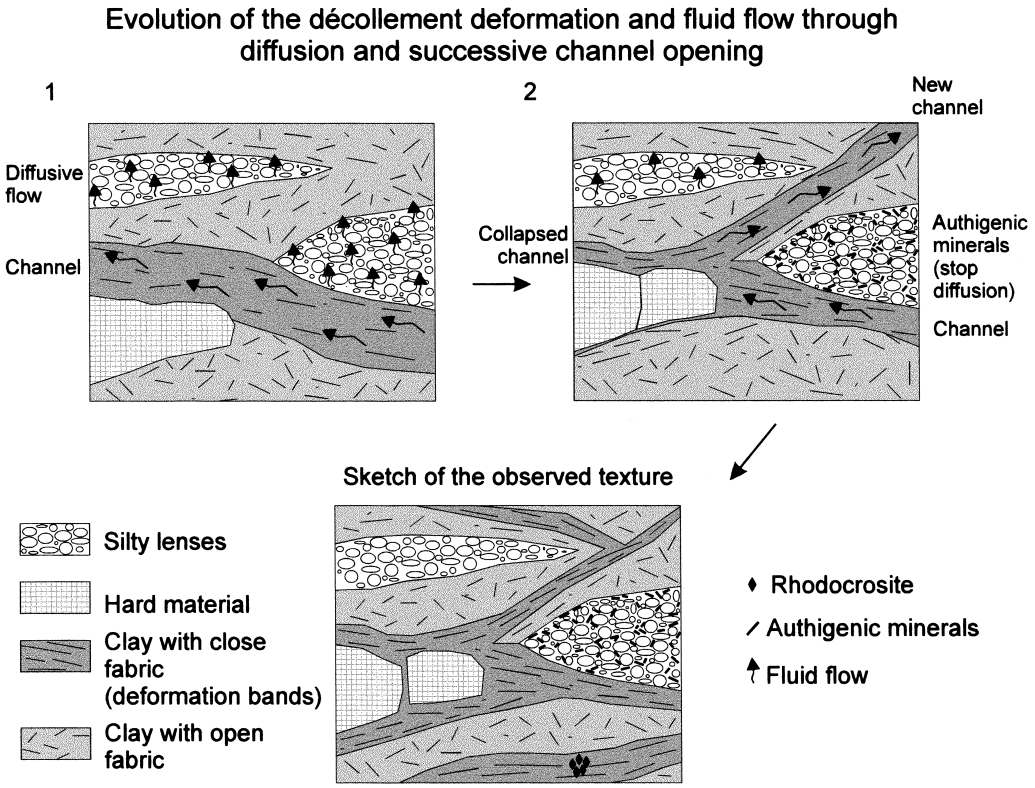

Fig. 9. Diagram of the décollement zone deformation history and hydrologic regime as interpreted from microstructural analyses.

tering is mainly channelled, and this may induce episodes of overpressuring related to zones of high clay content and low permeability that act as barriers.

Finally, moving from mesoscopic to microscopic scale reveals that the décollement maintains a self-similar appearance. The brittle blocks separated by thin horizons of ductile to semi-ductile material described at the core scale are still present at the microscale (Fig. 8a, b) at least down to the edge of the ductile décollement zone (Fig. 9). The boundary between the brittle and the ductile domains of the décollement zone, therefore, has a high potential to transmit fluids, since it combines brittle mechanisms, such as brecciation, with ductile ones such as the dilation of clay-rich horizons. This interpretation is in agreement with the localisation of the major fluid channel exactly in this boundary zone, as shown by anomalies in porewater geochemistry data (Kimura et al., 1997). The authigenic minerals in the ductile part of the décollement are evidence that fluid flow has occurred there, because their chemistry is not compatible with derivation from the local sediment.

4.3. Underthrust section

4.3.1. Core-scale observations

The underthrust section represents the same lithological sequence as the reference site 1039 (Fig. 2). From top to bottom, the first unit is a clayey diatomite (Unit U1, middle–upper Pleistocene), underlain by silty claystone (Unit U2, upper Miocene–middle Pleistocene) and then chalk (Unit U3, middle–upper Miocene). The lowest rocks encountered are intrusive pyroxene gabbros (Unit U4, ~15 Ma, K/Ar datum, J. Griffin, personal communication, for a complete description see Kimura et al., 1997).

Core-scale observations of the underthrust section have two important implications: the first concerns the amount of material lacking from the incoming Cocos plate, the second concerns the lithification state of the underthrust section in comparison with that at the reference site.

Based on comparison with the reference site (Kimura et al., 1997), the amount of material lacking from the top of Site 1040 underthrust section is about 10 m. This uppermost sediment could have been offscraped or simply eroded by bottom currents (Silver et al., 1997). The thickness and porosity of the underthrust section quantify the compaction experienced by these sediments as they are thrust beneath the wedge. The compaction is different for the different units. Based on lithostratigraphy, log data and porosity measurements at site 1040, unit U1 has undergone a volume loss of 34.73% and unit U2 of 14.66% relative to site 1039 (Fig. 2; Kimura et al., 1997).

The style of deformation abruptly changes from the décollement to the underthrust section. The ductile deformation of the lower part of the décollement is replaced downward by undeformed to brittlely deformed sediments in which sedimentary structures including burrows are well preserved. At site 1043 the sediments immediately beneath the décollement show some minor faulting, while at site 1040 they are completely undeformed. Faults in the underthrust section are morphologically quite different from those in the deformed sedimentary wedge. Typically in the underthrust section faults are discrete, narrow structures or braided arrays, and are never associated with ductile structures in the surrounding sediments. Offsets show that in the upper part of the underthrust section, where bedding dips show some scatter, faults are mainly reverse. This trend is interpreted as an effect of subduction and may imply some partitioning of lateral shortening below the décollement or incipient underplating. Toward the base of the underthrust section, the total number of faults tends to decrease, the proportion of normal faults increases, and bedding dips cluster about an average of 10–15°. The fault frequency and types in this lower sequence resemble those found at site 1039 (Kimura et al., 1997). Unit U3 (3 in the reference site) is characterised by liesegang coloration, cut and offset by small faults. Some sediment-filled veins and injections were also recovered.

The deformation style changes again at the very bottom of the underthrust section near the contact with the gabbro, where sedimentary breccia and slumped material was recovered (Kimura et al., 1997). Pinch-and-swell and boudinaged layers, normal faulting, incipient stylolitisation parallel to layers, and fluid escape structures are all features that indicate layer-parallel extension or layer-perpendicular flattening in this unit.

4.3.2. Microscopic observations

Samples from unit U1 are well compacted, with clay minerals draped around silt grains. Bioturbation is demonstrated by numerous burrows and the bedding is well oriented (dipping up to 40°). Unbroken microfossils are common. Some horizons show systems of parallel deformation bands and microfaults with reverse offsets. The bands are usually only 2–3 mm long and 0.1–1 mm thick and are steeply dipping with respect to bedding (Fig. 10). Why deformation bands and microfaults only cluster in certain layers is not clear; there is no evidence for control by grain size or degree of compaction. The morphology of deformation bands and microfaults can be anastomosing or discrete, and in the latter case they are thin. Thick bands contain silt grains, which, after an estimated rotation relative to the band edge of 45–50° on average, are now oriented parallel to the band edges. Toward the bottom of unit U1, smectites increase in abundance

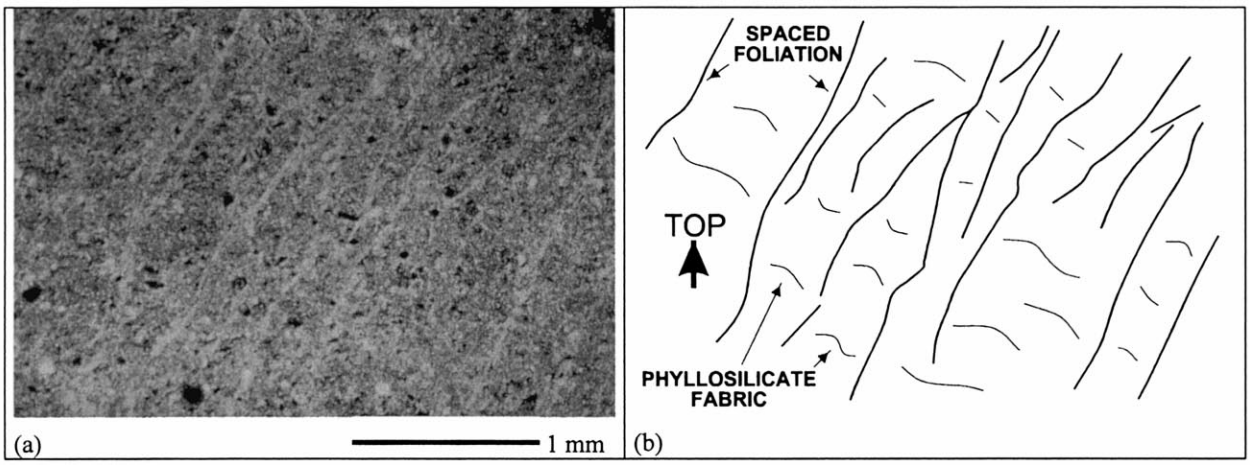

Fig. 10. Underthrust section: (a) Micrograph showing a spaced foliation. (b) Line drawing of (a) showing the offsets.

and in places form the bulk of the clay minerals. Pyrite-filled fractures are also present together with unflattened pyrite framboids.

Faults in Unit U2 are less numerous, but generally better developed in terms of length and thickness than those in unit U1. U2 faults can be several centimetres long and are detectable mesoscopically. They show a strong clay mineral orientation and lineated surfaces. The general fabric orientation is not well developed at the top of the unit but increases toward the bottom, where microfossils are sometimes broken and flattened parallel to bedding.

The top of unit U3 is almost undeformed, but contains some faults similar to those described for unit U2. Most of unit U3 is nearly completely undeformed except by compaction. In contrast, toward its base, U3 is extensively deformed. This deformation is very similar, in terms of style and degree, as that observed in the same unit at the reference site. The fabric shows very low porosity, and both silty grains and microfossils are oriented parallel to bedding. Microfossils are not broken, and very delicate features (e.g. foraminifer spines) are preserved in samples from the base of the unit (Fig. 11b). At the base of both sites 1040 and 1039, calcite and silica are present as neomorphic crystals on microfossil and grain surfaces. The neomorphic crystals have been precipitated syntaxially in cavities and are strain free. This recrystallisation is not continuous throughout the base of the sections. At site 1039, where the samples are more closely spaced, and the deformed sedimentary wedge is missing, the crystallisation of neomorphic crystals starts to be evident at 375.94 mbsf (Fig. 11a), although samples from 411.70 mbsf are not recrystallised (Fig. 11b). Where

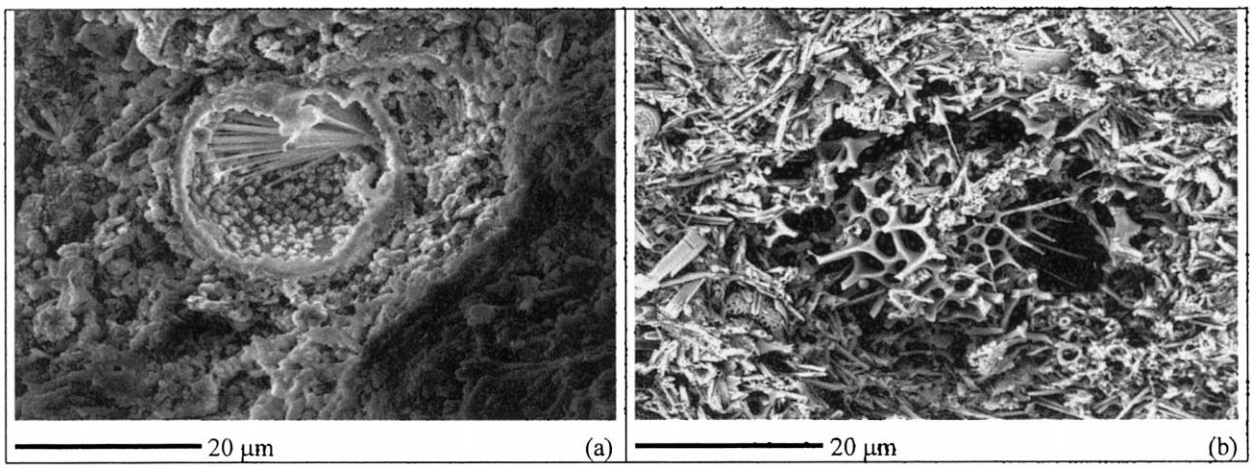

Fig. 11. Underthrust section: (a) Secondary SEM image of a recrystallised microfossil with calcite and quartz needles (sample from 411.70 mbsf, site 1040). (b) Backscattered SEM image of a radiolarian still with attached spines (sample from 421.62 mbsf, site 1040).

recrystallisation is evident, silty grains are generally surrounded by calcite, which may also form a patchy, incipient cementation.

4.3.3. Kinematic model of underthrust section deformation

The underthrust section shows two different deformation styles, one affecting Units u1, u2 and the first few metres of Unit u3 (underthrust style) and the other one characterising the lower part of unit U3 (basal style).

The parallel, very narrow deformation bands in certain layers from the top of the underthrust section are similar to the spaced foliation described by Labaume et al. (1997) as a microstructure associated with scaly fabric development in the Barbados accretionary prism. Maltman (pp. 426–429 in Borradaile et al., 1982) observed the same kinds of structures in laboratory experiments. The presence of regularly spaced bands in specific horizons suggests that strain was localised (Fig. 10). In addition the geometry is very similar to that of the mud-filled veins described by Hanamura and Ogawa (1993) and Brothers et al. (1996), who interpreted them as caused by seismic shaking. Seismic shaking causes opening of voids and liquefaction of the clays that surround them, which flow in and fill the voids. In the spaced foliation case, seismic shaking may cause the voids to open and close with no liquefaction, but with flattening of the clay minerals at the void edge.

The other structures representing the underthrust style are deformation bands and microfaults similar to those in the deformed sedimentary wedge. The higher concentration of deformation features in the upper part of the underthrust section is concordant with the higher porosity loss of unit U1 compared to unit U2. Magnetic fabrics show that this part of the section exhibits more flattening than the lower part (T. Kanamatsu, personal communication).

The basal style is interpreted as early-developed structures, partly inherited from features developed during Cocos plate evolution. The normal faulting is interpreted to be due to near-ridge tectonic processes. The faults occur after formation of the liesegangs, which result from alteration by fluids.

The abundant recrystallisation may be the product of silica and calcium carbonate mobilisation due to pressure-solution, as indicated by incipient stylolitisation, or could derive from a distant source. Geochemical data (Kimura et al., 1997) show that silica reaches saturation with respect to opal A at about 300 mbsf at site 1039 and that at about 400 mbsf, the silica content drops steeply, although diatoms are still abundant. The same trend is shown at the same relative depths at sites 1040. The silica decrease could be the result of fluid communication with a low-silica source or interaction with the underlying gabbro (Kimura et al., 1997). The mobilisation of silica and calcium carbonate has two different signatures as the bottom of the sedimentary section (and the gabbro intrusion) is approached. At 20 m above the gabbro, quartz and calcite precipitate, while near the gabbro they do not. This behaviour can be explained by assuming a different and separate fluid circulation regime connected with the gabbro. The basal style of deformation allows the elimination of the silica and the calcium carbonate (undersaturation?) so that they cannot precipitate.

5. Conclusions

Core-scale and microscopic analyses of the two lower slope sites drilled in the Costa Rica subduction complex reveal four structural/hydrologic regimes.

The deformation in the sedimentary wedge is influenced by the relative increasing value of the maximum principal stress alternating in orientation between vertical and horizontal, together with transient pulses of increased pore pressure. This mechanism has been previously proposed elsewhere (Byrne et al., 1993), but Costa Rica presents new data and an enlarged view of the processes that build up convergent margins. We suggest that at shallow levels of the wedge, where gravitational loading stresses predominate over sub-horizontal compression, transient pore pressure regimes opened channels, increasing permeability and rate of dewatering. Channel collapse and alignment of clay mineral particles producing local densification of the sediments followed. Eventually, in the deeper level of the wedge, a stable bulk tectonic stress with a sub-horizontal maximum principal stress was established. This regime and an increasing amount of shear strain acting on denser sediments, permitted development of channels of concentrated fluid flow. The dewatering and compaction would tend to decrease the likelihood of large pore pressure fluctuation and produce lithification, so later stage deformation features are fractures and microfaults.

The décollement zone is characterised by a heterogeneous grain size distribution, deformation style and clay mineral fabric. Lenses of silt alternate with clay-rich horizons, and form permeable zones, which allowed microscale local diffusive flow but are surrounded by impermeable zones. Lithification is heterogeneous and deformation bands surround well compacted, slightly cemented and brittlely deformed domains. This domainal structure defines a hydraulic breccia, in which the dimensions of the clasts decrease toward the base of the décollement zone, where they lose their brittle character and may deform plastically. Deformational structures are still compatible with a strain regime within which transient episodes of high

pore pressure produced dilation. Because of the coupled volume–pore pressure fluctuations, the dewatering process could have been most effectively carried out through sediments that show a combination of brittle and ductile deformation styles, typical of deformation at critical state (Bolton et al., 1998). Porewater geochemistry indicates the major fluid conduit is within the décollement zone (Kastner et al., 1997).

The underthrust section is decoupled from the wedge and the décollement zone in terms of its deformation history. There is no evidence of discrete fluid conduit structures on the core scale supplying fluids from the underthrust sediments to the décollement. It is likely that fluids are collected and brought to the décollement by way of major fault discontinuities away from the drill site, detected in the seismic profile (Kimura et al., 1997). Major fault discontinuities are likely to behave as discrete fluid conduits. Compared to the reference site, the underthrust section records greater compaction. Sediments show parallel, equally spaced deformation bands occurring in specific layers, suggesting their origin is related to a periodic phenomenon, such as seismic shaking. In this scenario, supported by the high seismic activity of the margin, earthquakes may have enhanced the dewatering process.

The sediments just above the basal gabbro show a completely different structural style, related not to sediment dewatering, but to early near-ridge tectonic processes and a basal hydrologic system, as documented by geochemical data. The gabbro hydrologic system seems to be fed by a source of seawater composition.

Acknowledgements

We wish to thank all our Leg 170 colleagues, particularly Ben Clennell, and Alex Maltman for discussion on an earlier version of the paper. We are greatly indebted to Bianca Maria Cita, Paolo Fazzini and Isabella Premoli Silva, who support all the expenses of this research. Tobin acknowledges JOI/USSSP post-cruise science support. Reviews by Richard Norris, Evan Leitch and an anonymous referee are also acknowledged.

References

Bolton, A.J., Maltman, A.J., 1998. Fluid-flow pathways in actively deforming sediments: the role of fluid pressures and volume changes. Marine and Petroleum Geology 15, 281–297.

Bolton, A.J., Clennell, M.B., Maltman, A.J., 1999. Non-linear stress dependence of permeability: a mechanism for episodic fluid flow in accretionary prisms. Geology 27, 239–242.

Bolton, A.J., Maltman, A.J., Clennell, M.B., 1998. The importance of overpressure timing and permeability evolution in fine-grained sediments undergoing shear. Journal of Structural Geology 20, 1013–1022.

Borradaile, G.J., Bayly, M.B., Powell, C.McA., 1982. Atlas of Deformational and Metamorphic Rock Fabric. Springer–Verlag, Berlin.

Bray, J.C., Karig, D.E., 1985. Porosity of sediments in accretionary prisms and some implications for dewatering processes. Journal of Geophysical Research 90, 768–778.

Brothers, R.J., Kemp, A.E.S., Maltman, A.J., 1996. Mechanical development of vein structures due to the passage of earthquake waves through poorly consolidated sediments. Tectonophysics 260, 227–244.

Byrne, T., Maltman, A., Stephenson, E., Soh, W., Knipe, R., 1993. Deformation structures and fluid flow in the toe region of the Nankai accretionary prism. In: Hill, I.A., Taira, A., Firth, J.V. (Eds.), Proceedings of the Ocean Drilling Program, Scientific Results, pp. 83–101.

Dadey, K.A., Leinen, M., Silva, A.J., 1990. Anomalous stress history of sediments of the Northwest Pacific: the role of microstructure. In: Bennett, R.H., Bryant, W.R., Hulbert, M.H. (Eds.), Microstructure of Fine-grained Sediments, from Mud to Shale. Springer–Verlag, New York, pp. 229–236.

Hanamura, Y., Ogawa, Y., 1993. Layer-parallel faults, duplexes, imbricate thrusts and vein structures of the Miura Group: keys to understanding the Izu fore-arc sediment accretion to the Honshu fore-arc. The Island Arc 3, 126–141.

Hinz, K., Von Huene, R., Ranero, C.R., Working Group, PACOMAR, 1996. Tectonic structure of the convergent Pacific margin offshore Costa Rica from multichannel seismic reflection data. Tectonics 15, 54–66.

Jones, M.E., Addis, M.J., 1986. The application of stress path and critical state analysis to sediment deformation. Journal of Structural Geology 8, 575–580.

Kastner, M., Zheng, Y., Laier, T., Jenkins, W., Ito, T., 1997. Geochemistry of fluids and flow regime in the décollement zone at the northern Barbados Ridge. In: Shipley, T.H., Ogawa, Y., Blum, P., Bahr, J.M. (Eds.), Proceedings of the Ocean Drilling Program, Scientific Results, 156. Ocean Drilling Program, College Station, TX, pp. 311–319.

Kimura, G., Silver, E., Blum, P., Leg 170 Scientific Party, ODP, 1997. Proceedings of the Ocean Drilling Program, Initial Reports, 170. Ocean Drilling Program, College Station, TX.

Logan, J.M., Friedman, M., Higgs, N., Dengo, C., Shimamoto, T., 1979. Experimental studies of simulated gouge and their application to studies of natural fault zones. Open-File Report. US Geological Survey 79-1239, 305–343.

Lundberg, N, Moore, J.C., 1986. Macroscopic structural features in Deep Sea Drilling Project cores from forearcs. Geological Society of America Memoir 166, 13–44.

Maltman, A.J., 1998. Deformation structures from the toes of active accretionary prisms. Journal of the Geological Society of London 155, 639–650.

Maltman, A.J., Byrne, T., Karig, D.E., Lallemant, S., 1993. Deformation at the toe of an active accretionary prism: synopsis of results from ODP Leg 131, Nankai, SW Japan. Journal of Structural Geology 15, 949–964.

McAdoo, B., Orange, D., Silver, E., McIntosh, K., Abbott, L., Galewsky, J., Kahn, L., Protti, M., 1996. Seafloor structural observations, Costa Rica accretionary prism. Geophysical Research Letters 23, 883–886.

Scholl, D.W., Plank, T., Morris, J., Von Huene, R., Mottl, M.J., 1994. Science opportunities in Ocean Drilling to investigate recycling processes and material fluxes at subduction zones. In: Proceedings of a JOI/USSAC workshop, Avalon, 12–17 June, 1994.

Schoonmaker, J., Mackenzie, F., Manghani, M., Scheider, R., Kim,

D., Weiner, A., To, J., 1985. Mineralogy and diagenesis: their effect on acoustic and electrical properties of pelagic clays, Deep Sea Drilling Project Leg 86. In: Heath, G.R., Burckle, L.H., et al. (Eds.), Initial Reports of the Deep Sea Drilling Project, 86. US Government Printing Office, Washington DC, pp. 549–570.

Shipley, T.H., McIntosh, K.D., Silver, E.A., Stoffa, P.L., 1992. Three-dimensional seismic imaging of the Costa Rica accretionary prism: structural diversity in a small volume of the lower slope. Journal of Geophysical Research 97, 4439–4459.

Shipley, T.H., Ogawa, Y., Blum, P., Leg 156 Scientific Party, ODP, 1995. Proceedings of the Ocean Drilling Program, Initial Reports, 170. Ocean Drilling Program, College Station, TX.

Silver, E., Leg 170 Scientific Party, ODP, 1997. Complete sediment subduction and implications of fluid flow in the Middle America Trench off Costa Rica. Joides Journal 23/2, 1–3.

Smart, P., Tovey, N.K., 1981. Electron Microscopy of Soils and Sediments: Examples. Clarendon Press, Oxford.

Suppe, J., 1985. Principles of Structural Geology. Prentice Hall, New Jersey.

Teas, P.A., Tobin, H.J., García, P.E., 1995. Microstructural analysis of Sites 891 and 892: implications for deformation processes at the frontal thrust and an out-of-sequence thrust. In: Carson, B., Westbrook, G.K., Musgrave, R.J., Suess, E. (Eds.), Proceedings of the Ocean Drilling Program, Scientific Results, pp. 217–225.

Von Huene, R., Bialas, J., Flueh, E., Cropp, B., Fabel, E., Hoffmann, J., Emeis, K., Holler, P., Jeschke, G., Leandro, C., Perez Fernandez, I., Chavarria, J., Florez, H., Escobedo, D., Leon, R, Barrios, O., 1995. Morphotectonics of the Pacific convergent margin of Costa Rica. Geological Society of America Special Paper 295, 291–307.